A Semianalytical Model of Bilayer-Graphene Field-Effect Transistor

Martina Cheli, Gianluca Fiori, and Giuseppe Iannaccone, *Member, IEEE*

***Abstract*—Bilayer graphene has the very interesting property of an energy gap tunable with the vertical electric field. We propose an analytical model for a bilayer-graphene field-effect transistor, suitable for exploring the design parameter space in order to design a device structure with promising performance in terms of transistor operation. Our model, based on the effective mass approximation and ballistic transport assumptions, takes into account bilayer-graphene tunable gap and self-polarization and includes all band-to-band tunneling current components, which are shown to represent the major limitation to transistor operation, because the achievable energy gap is not sufficient to obtain a large I_{on}/I_{off} ratio.**

***Index Terms*—Analytical model, band-to-band tunneling, field-effect transistors (FETs), graphene bilayer.**

I. Introduction

THE PROGRESS of CMOS technology, with the pace foreseen by the International Technology Semiconductor Roadmap (ITRS) [1], cannot be based only on the capability to scale down device dimensions, but requires the introduction of new device architectures [2] and new materials for the channel, the gate stack, and the contacts. This trend has already emerged for the recent technology nodes and will hold—probably requiring more aggressive innovations—for devices at the end of the Roadmap.

In the last decade, carbon allotropes have attracted the attention of the scientific community, first with carbon nanotubes [3] and, since its isolation in 2004, with graphene [4], which has shown unique electronic [5] and physical properties [6], such as unconventional integer quantum Hall effect [7], [8], high carrier mobility [4] at room temperature, and potential for a wide range of applications [9]–[11], like nanoribbon FETs [12]. Despite of the fact that graphene is a zero gap material, an energy gap can be engineered by "rolling" it in carbon nanotubes [13] or by the definition of lateral confinement like in graphene nanoribbons [14]. However, theoretical [15] and experimental [16] works have shown that a significant gap in nanoribbons is obtained for widths close to 1–2 nm, which are prohibitive for fabrication technology on the scale of integrated circuits, at least in the medium term.

Recently, theoretical models [17]–[19] and experiments [20] have shown that bilayer graphene has the interesting property of an energy gap tunable with an applied vertical electric field. Anyway, the largest attainable gap is of a few hundreds of millielectronvolts, which make its use questionable for nanoelectronic applications: Limits and potentials of bilayer graphene still have to be shown.

From this point of view, device simulations can greatly help in assessing device performance. Bilayer-graphene field-effect transistors (BG-FETs) have been compared against monolayer FETs, by means of the effective mass approximation [21] and Monte Carlo simulations [22] in the ballistic limit, showing really poor potential as compared to ITRS requirements [1]. These approaches, however, did not take into account some of the main specific and important properties of bilayer graphene, such as the possibility of tuning the band gap and the dispersion relation with the vertical electric field and dielectric polarization in the direction perpendicular to the 2-D sheet. Such problems have been overcome in [23], using a real-space tight-binding (TB) approach. However, for the limited set of device structures considered, the small band gap does not allow a proper on and off switching of the transistor.

One limitation of detailed physical simulations is that, despite their accuracy, they are typically too demanding from a computational point of view for a complete investigation of device potential. Analytical approaches could help in this case. One example has been proposed in [24], but it has serious drawbacks, because it completely neglects band-to-band tunneling and the dependence of the effective mass on the vertical electric field, providing an unrealistically optimistic picture of the achievable performance.

In this paper, we have developed a semianalytical model for a bilayer-graphene FET with two gates to study the possibility of realizing a FET by tuning the gap with a vertical electric field. The model has been validated through comparison with results obtained by means of our full 3-D atomistic Poisson–Schrödinger solver NanoTCAD ViDES [25], showing good agreement in the applied bias range [23]. Interband tunneling proves to be the main limiting factor of device operation, as demonstrated by the device analysis performed in the parameter space.

II. Model

In this section, we provide a detailed description of the developed model, which is based both on a top of the barrier

Manuscript received September 9, 2009. First published October 30, 2009; current version published November 20, 2009. This work was supported in part by the EC Seventh Framework Program through Project GRAND under Contract 215752 and in part by the Network of Excellence NANOSIL under Contract 216171. The review of this paper was arranged by Editor M. Reed.

The authors are with the Dipartimento di Ingegneria dell'Informazione: Elettronica, Informatica, Telecomunicazioni, Università degli Studi di Pisa, 56100 Pisa, Italy (e-mail: martina.cheli@iet.unipi.it; gfiori@mercurio.iet.unipi.it; g.iannaccone@iet.unipi.it).

Color versions of one or more of the figures in this paper are available online at http://ieeexplore.ieee.org.

Digital Object Identifier 10.1109/TED.2009.2033419

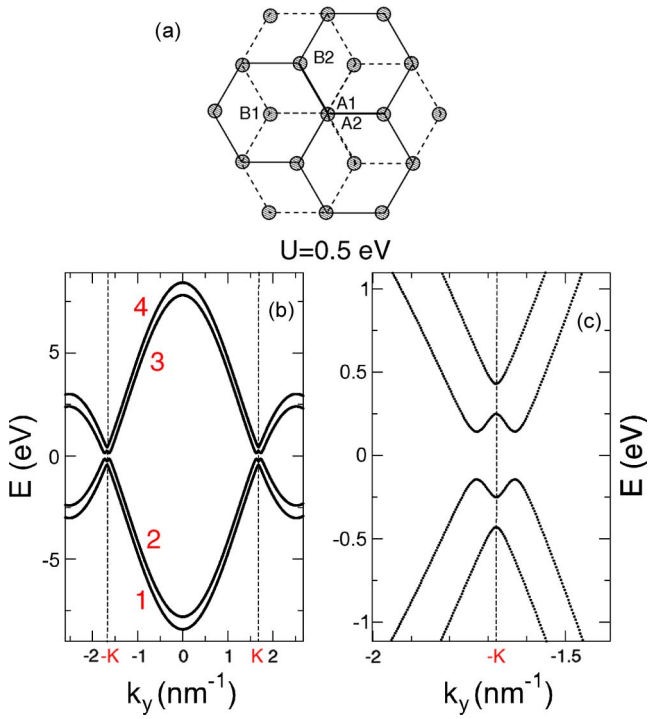

Fig. 1. (a) Real-space lattice structure of bilayer graphene. The bilayer consists of two coupled hexagonal lattices with inequivalent sites A1, B1 and A2, B2 in the first and second sheets, respectively, arranged according to Bernal (A2–B1) stacking. (b) TB band structure of bilayer graphene for $U = U_1 - U_2 = 0.5$ eV. (c) Detail of the band structure in correspondence of band minimum $k_{\min}$: K is the Dirac point.

model [26] and on the calculation of all the interband tunneling components. In particular, we adopt the ballistic transport and the effective mass approximation, whose main physical parameters, such as the effective mass and the energy gap, have been extracted from the energy bands obtained from a p_z-orbital TB Hamiltonian. Since we want to address long-channel devices, short-channel effects have been completely neglected, as well as inelastic scattering mechanisms, which are expected to be negligible in this kind of material [6]. With respect to more accurate atomistic models, the followed approach may underestimate the actual concentration of carriers in the channel, particularly for large drain-to-source ($V_{\rm DS}$) and gate ($V_{\rm GS}$) voltages, when a parabolic band misses to match the exact dispersion relation. However, we believe that the developed model represents a good tradeoff between accuracy and speed.

A. Effective Mass Approximation

In order to proceed with the definition of an analytical model based on the effective mass approximation, we first need an expression for the energy bands of bilayer graphene. The top view of the bilayer-graphene lattice structure with carbon–carbon distance $a = 1.44$ Å is shown in Fig. 1(a): A1–B1 atoms lay on the top layer, while A2–B2 atoms lay on the bottom layer. The energy dispersion relation can be computed by means of a p_z-TB Hamiltonian [27] considering two layers of graphene coupled in correspondence of the overlaying atoms A1 and A2. The energy dispersion relation reads [17]

$$E(\mathbf{k}) = \frac{U_1+U_2}{2} \pm \sqrt{|f(\mathbf{k})|^2 + \frac{U^2}{4} + \frac{t_\perp^2}{2} \pm \frac{1}{2}\sqrt{4\left(U^2+t_\perp^2\right)|f(\mathbf{k})|^2 + t_\perp^4}} \tag{1}$$

where U_1 and U_2 are the potential energies on the first and second layers, respectively, $U = U_1 - U_2$, $t_\perp = -0.35$ eV is the interlayer hopping parameter [17], $\mathbf{k} = k_x\hat{k}_x + k_y\hat{k}_y$, and [27]

$$f(\mathbf{k}) = te^{ik_x a/2}\left[2\cos\left(\frac{k_y a\sqrt{3}}{2}\right) + e^{-i3k_x a/2}\right] \tag{2}$$

is the well-known off-diagonal element of the 2×2 graphene p_z-Hamiltonian, where t is the in-plane hopping parameter ($t = -2.7$ eV). In Fig. 1(b), the band diagram for $U = 0.5$ eV is shown. As can be seen, bilayer graphene has four bands, which are symmetric with respect to the coordinate axis. For large U values, the "mexican-hat" behavior in correspondence of the band minima can be observed, as shown in Fig. 1(c).

Let us now consider the third band [Fig. 1(b)], which corresponds to the conduction band (same considerations follow for the valence band, i.e., second band), and apply a parabolic band approximation in correspondence of the minimum $k_{\min}$, which reads [17]

$$k_{\min} = \sqrt{\frac{U^2+2t_\perp^2}{U^2+t_\perp^2}}\frac{U}{2v_F\hbar}. \tag{3}$$

The dispersion relation can now be expressed as [17]

$$E(\mathbf{k}) = \frac{E_{\rm gap}}{2} + \frac{\hbar^2}{2m^*}\left(|\mathbf{k}| - k_{\min}\right)^2 + \frac{U_1+U_2}{2} \tag{4}$$

where

$$m^* = \frac{t_\perp\left(U^2+t_\perp^2\right)^{3/2}}{2U\left(U^2+2t_\perp^2\right)}\frac{1}{v_F^2}; \quad E_{\rm gap} = \frac{Ut_\perp}{\sqrt{U^2+t_\perp^2}}. \tag{5}$$

$v_F = (3at/2\hbar)$ is the Fermi velocity, and $\hbar$ is the reduced Planck's constant.

As can be observed in (5), the effective mass m^* has a singularity for $U = 0$, which is clearly unphysical. In order to avoid such an issue, energy bands in the range $U \in [0, 0.14]$ have been fitted with the parabolic expression in (4), within an energy range of $2k_B$T from the band minimum (where k_B is the Boltzmann constant and T is the room temperature), and using m^* as a fitting parameter. In Fig. 2(a) and (b), we show, for two different interlayer potential energies ($U = 0$ eV and $U = 0.1$ eV), the TB energy bands as well as the parabolic bands exploiting the analytical expression in (5) and the fitted values for m^*, respectively. As can be seen, the fitted effective mass manages to better match the TB band in the specified energy range. In Fig. 2(c), we show the fitted effective mass

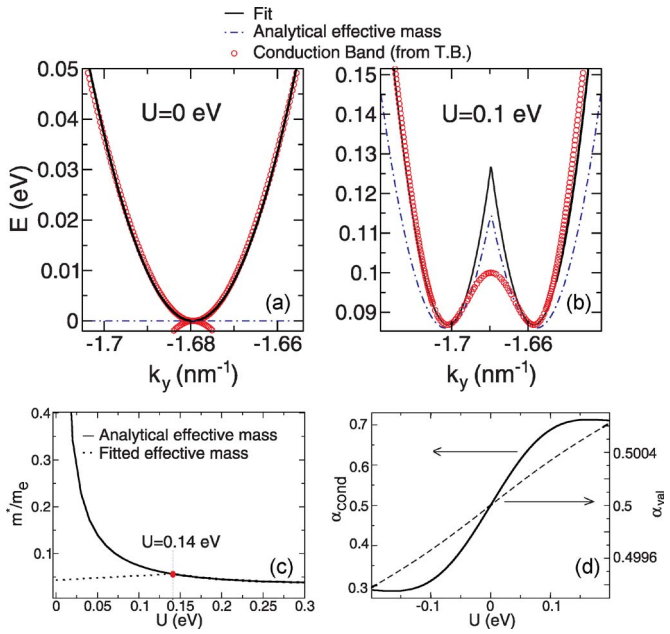

Fig. 2. Comparison between energy dispersions obtained by means of the (dashed–dotted line) analytical effective mass, (solid line) fitted effective mass, and (circle) TB Hamiltonian for an interlayer potential equal to (a) $U = 0$ eV and (b) $U = 0.1$ eV. (c) Analytical and fitted relative effective mass as a function of the interlayer potential U. m_e is the free electron mass. (d) $\alpha_{\rm cond}(U)$ and $\alpha_{\rm val}(U)$ as a function of the interlayer potential U.

for different U. In particular, for $U < 0.14$ eV, m^* can be written as

$$\frac{m^*}{m_e} = 0.09U + 0.043 \tag{6}$$

where m_e is the electron mass at rest and U is expressed in eV. For larger values of U, (5) is recovered.

B. Electrostatics

Once obtained the expression for m^*, the electron concentration n can be expressed as

$$n = \frac{\nu}{2}\int_{E_c}^{+\infty} D(E)\left[f(E-E_{\rm FS}) + f(E-E_{\rm FD})\right]dE \tag{7}$$

where f is the Fermi–Dirac occupation factor, $E_{\rm FS}$ and $E_{\rm FD}$ are the Fermi energies of the source and drain, respectively, and $\nu = 2$ is the band degeneracy. $D(E)$ is the total density of states per unit area (for the complete calculation, see the Appendix), which reads

$$D(E) = \frac{1}{2\pi\hbar}\left(\frac{2m^*}{\hbar} + \sqrt{\frac{2m^*}{E-E_c}}k_{\rm min}\right) \tag{8}$$

where E_c is the conduction band edge. If we define

$$f_n(E_f) = \frac{m^*}{\pi\hbar^2}k_BT\ln\left[1+\exp\left(\frac{E_c-E_f}{k_BT}\right)\right] + \frac{k_{\rm min}\sqrt{2m^*k_BT}}{2\pi\hbar}F_{1/2}\left(\frac{E_c-E_f}{k_BT}\right) \tag{9}$$

where $F_{1/2}$ is the Fermi–Dirac integral of order 1/2, the electron concentration reads

$$n = \left[f_n(E_{\rm FS}) + f_n(E_{\rm FD})\right]. \tag{10}$$

Analogous considerations can be made for the hole concentration p, which reads

$$p = \left[f_p(E_{\rm FS}) + f_p(E_{\rm FD})\right] \tag{11}$$

where

$$f_p(E_f) = \frac{m^*}{\pi\hbar^2}k_BT\ln\left[1+\exp\left(\frac{E_f-E_v}{k_BT}\right)\right] + \frac{k_{\rm min}\sqrt{2m^*k_BT}}{2\pi\hbar}F_{1/2}\left(\frac{E_f-E_v}{k_BT}\right) \tag{12}$$

and E_v is the valence band edge.

Once n and p are computed, attention has to be posed on how charge distributes on the two layers, i.e., on dielectric polarization. To this purpose, we have numerically extracted, from TB simulations, $\alpha_{\rm val}(U)$ and $\alpha_{\rm cond}(U)$, which represent the fractions of the total states in the valence band and of electrons in the conduction band, respectively, on layer 1 [23]. We computed $\alpha_{\rm cond}(U)$ for a particular bias ($U_1 = -U_2 = U/2$ and $E_F = 0$ eV) and made the assumption that its dependence on the bias can be neglected. As far as $\alpha_{\rm val}$ is concerned, we assumed, in our considered bias range, that all electron states in the valence band are fully occupied, and therefore, $f(E) = 1$. Fig. 2(d) shows $\alpha_{\rm cond}(U)$ and $\alpha_{\rm val}(U)$ as a function of the interlayer potential U. The charge density ρ_j per unit area on layer j ($j = 1, 2$) is expressed as the sum of the polarization charge, electrons, and holes and finally reads

$$\begin{aligned}\rho_1(U) &= q\left\{\left[1-2\alpha_{\rm val}(U)\right]N_{\rm tot} - n\left[1-2\alpha_{\rm cond}(U)\right] + p\alpha_{\rm cond}(U)\right\}\\ \rho_2(U) &= q\left\{\left[2\alpha_{\rm val}(U)-1\right]N_{\rm tot} - n\alpha_{\rm cond}(U) + p\left[1-2\alpha_{\rm cond}(U)\right]\right\}\end{aligned} \tag{13}$$

where q is the electron charge and $N_{\rm tot}$ is the concentration of ions per unit area.

The considered device structure is a double-gate FET embedded in SiO_2. The bilayer graphene interlayer distance d is equal to 0.35 nm, while two different oxide thicknesses t_1 and t_2 have been considered [Fig. 3(a)]. An air interface between bilayer graphene and oxide has also been taken into account ($t_{\rm sp} = 0.5$ nm) [28]. For such a system, we can define an equivalent capacitance circuit as in Fig. 3(b), where $C_0 = (\epsilon_0/d)$, $C_1 = [(t_1/\epsilon_1) + (t_{\rm sp}/\epsilon_0)]^{-1}$, $C_2 = [(t_2/\epsilon_2) + (t_{\rm sp}/\epsilon_0)]^{-1}$, and $\epsilon_1 = \epsilon_2 = 3.9\epsilon_0$, while $\epsilon_0 = 8.85 \times 10^{-12}$ F/m. $V_{\rm Tg}$ and $V_{\rm Bg}$ are the top- and back-gate voltage, respectively, $V_1 \equiv (-U_1/q)$, and $V_2 \equiv (-U_2/q)$. In Fig. 3(c), the flat-band diagram along the transverse direction (y axis) is shown. Metal work functions for the back and top gates are equal to 4.1 eV [$\Phi_{\rm Bg} = \Phi_{\rm Tg} = 4.1$ eV], while the graphene work function ($\Phi_{\rm gra}$) is equal to 4.5 eV [29]. $\rm E_{FTg}$ and $\rm E_{FBg}$ are the Fermi level of the top and back gates, respectively.

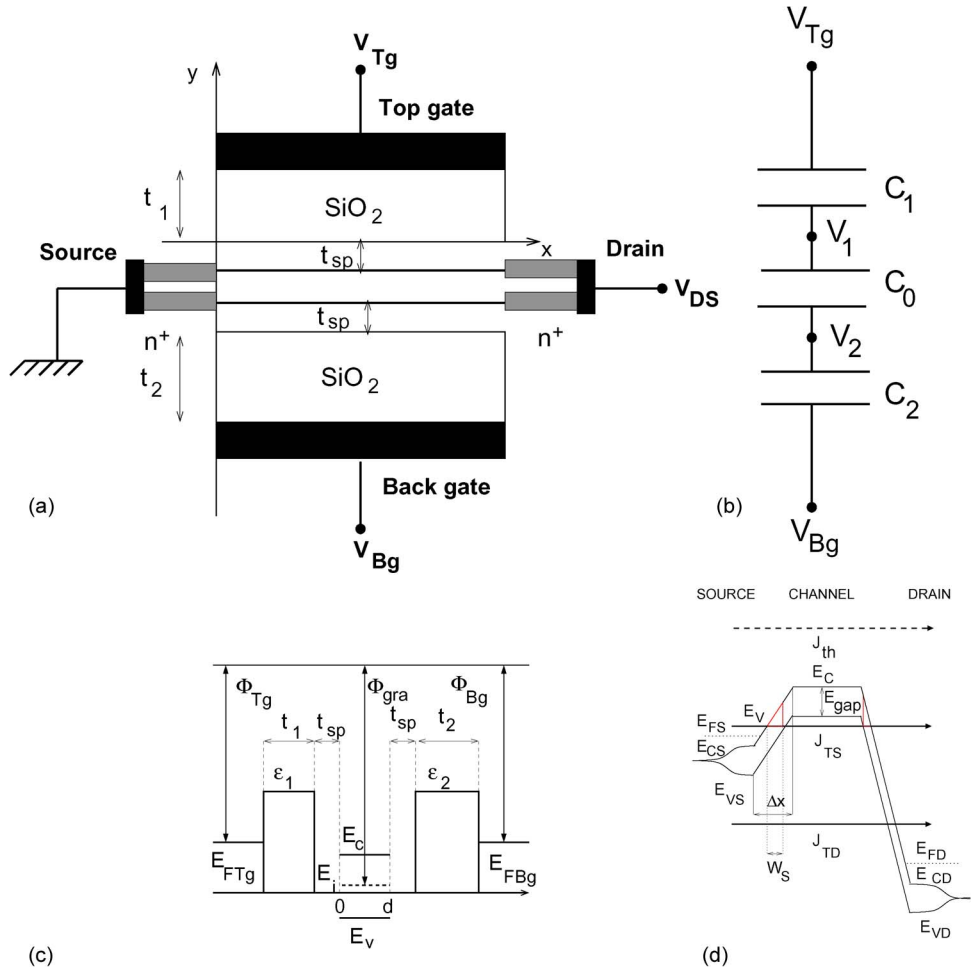

Fig. 3. (a) Sketch of the considered BG-FET: d is the interlayer distance, and t_1 and t_2 are the top and back oxide thicknesses. (b) Equivalent capacitance circuit of the simulated device. (c) Flat-band diagram of the BG-FET along the y-direction. (d) Conduction and valence band edge profiles in the longitudinal direction; we assume that, deep in the source and drain regions, the electric field induced by the gate vanishes and that the gap gradually reduces to zero.

The conduction band edge inserted in (9) can be expressed as

$$E_c = \Phi_{\rm Bg} + E_{\rm FBg} - \Phi_{\rm gra} + \frac{U_1 + U_2}{2} + \frac{E_{\rm gap}}{2}. \tag{14}$$

Applying the Gauss theorem, we obtain the following:

$$\begin{cases} C_1(V_{\rm Tg} - V_1) + (V_2 - V_1)C_0 = -\rho_1 \\ C_0(V_1 - V_2) + (V_{\rm Bg} - V_2)C_2 = -\rho_2. \end{cases} \tag{15}$$

Equations (13) and (15) are then solved self-consistently until convergence on V_1 and V_2 is achieved.

C. Current

Drain-to-source ($J_{\rm TOT}$) current is computed at the end of the self-consistent scheme. As shown in Fig. 3(d), $J_{\rm TOT}$ consists of three different components: The first is due to the thermionic current $J_{\rm th}$ over the barrier [26], whereas the second ($J_{\rm TS}$) and the third ($J_{\rm TD}$) are due to band-to-band tunneling. In the same figure, we show the conduction band edge $E_{\rm CS}$ ($E_{\rm CD}$) and the valence band edge $E_{\rm VS}$ ($E_{\rm VD}$) at the source (drain). Assuming reflectionless contacts, the thermionic current is due to electrons injected from the source with positive velocity $v_x > 0$ and to electrons injected from the drain with $v_x < 0$

$$J_{\rm th} = \frac{-q}{\pi^2\hbar}\int_{-\infty}^{+\infty} dk_y \left[\int_{k_x^>} \frac{\partial E}{\partial k_x} f(E - E_{\rm FS}) dk_x + \int_{k_x^<} \frac{\partial E}{\partial k_x} f(E - E_{\rm FD}) dk_x \right] \tag{16}$$

where $E = E_c + (\hbar^2/2m^*)(|\mathbf{k}| - k_{\rm min})^2$, $v_x = (1/\hbar)(\partial E/\partial k_x)$ is the group velocity, and $k_x^>$ ($k_x^<$) is the wave vector range for which $v_x > 0$ ($v_x < 0$). For the complete derivation, see the Appendix.

Let us now discuss the band-to-band tunneling current due to the barrier at source (drain) contact, which reads

$$J_{Ti} = 2\int_{k_y}\int_{k_x^>} q\frac{1}{2\pi^2}\frac{1}{\hbar}\frac{\partial E}{\partial k_x} T_i(k_y) \times \left[f(E - E_{\rm FS}) - f(E - E_{\rm FD})\right] \partial k_x \partial k_y, \qquad i = S, D \tag{17}$$

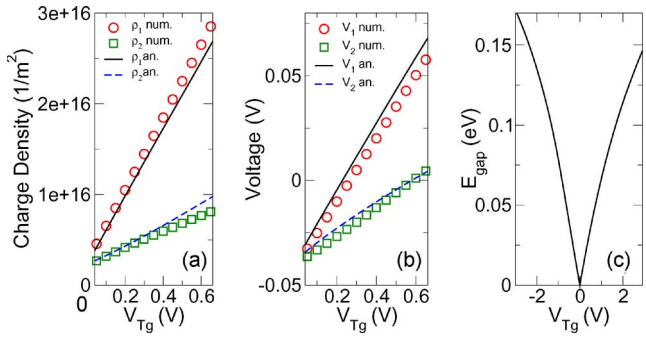

Fig. 4. Comparison between analytical and numerical simulations of (a) ρ_1 and ρ_2 and (b) V_1 and V_2 as a function of $V_{\rm Tg}$. $V_{\rm Bg} = 0$ V and $V_{\rm DS} = 0$ V. (c) Energy gap as a function of top-gate voltage, with $V_{\rm Bg} = 0$ V.

where S refers to the source and D refers to the drain, while $T_i(k_y)$ is the transmission coefficient at the different reservoirs. The key issue in computing (17) is the definition of an expression for $T_i(k_y)$, which accounts for the band-to-band tunneling process.

We have assumed a non-charge-neutrality region of fixed width Δx at the contact/channel interface and an electric field $\mathcal{E}_i = (E_c - E_{\rm Fi})/(q\Delta x)$ with $i = S, D$. For what concern the $J_{\rm TS}$ term, electrons emitted with electrochemical potential $E_{\rm FS}$ see two triangular barriers, one at the source junction and one in correspondence of the drain [Fig. 3(d)], whose heights are equal to $E_{\rm gap}$ and widths are $W_i = E_{\rm gap}/(q\mathcal{E}_i)$. Assuming the same Δx for both source and drain junctions, the drain barrier is transparent with respect to the source barrier, since, for large $V_{\rm DS}$ values, the electric field at the source is smaller than the electric field at the drain barrier: $T_S(k_y)$ is therefore essentially given by the source junction barrier. The same considerations follow for the other band-to-band tunneling current component $J_{\rm TD}$, flowing only through the drain-channel contact. In this case, $\mathcal{E} = E_c - E_{\rm FD} = (E_c - E_{\rm FS} + qV_{\rm DS})/(q\Delta x)$.

Assuming the WKB approximation, the transmission coefficient can be expressed as

$$T_i(k_y) = e^{-2\int_{[W_b]} |Im\{k_x\}|dx}, \qquad i = S, D \tag{18}$$

where $\mathrm{Im}\{k_x\}$ is the imaginary part of k_x and is obtained from

$$\frac{\hbar^2}{2m^*}\left(|\mathbf{k}| - k_{\rm min}\right)^2 = q\mathcal{E}_i x - E_{\rm gap}, \qquad i = S, D. \tag{19}$$

Finally, $J_{\rm Ti}$ is computed by performing the integral (17) numerically.

III. Exploration of the Design Space

In order to validate our model, we have first compared analytical results with those obtained by means of numerical NEGF TB simulations [25], considering a test structure with $t_1 = t_2 = 1.5$ nm, $t_{\rm sp} = 0.5$ nm, $\Phi_{\rm gra} = \Phi_G = \Phi_{\rm Bg} = 4.1$ eV, $V_{\rm DS} = 0.1$ V, and $V_{\rm Bg} = 0$ V. In Fig. 4(a)–(b), the electron concentrations (ρ_1, ρ_2) and the electrostatic potentials (V_1, V_2) on layers 1 and 2 are shown, as a function of $V_{\rm Tg}$, for $V_{\rm DS} = 0$ V and $V_{\rm Bg} = 0$ V. As can be seen, results are in good agreement. Some discrepancies, however, occur for larger

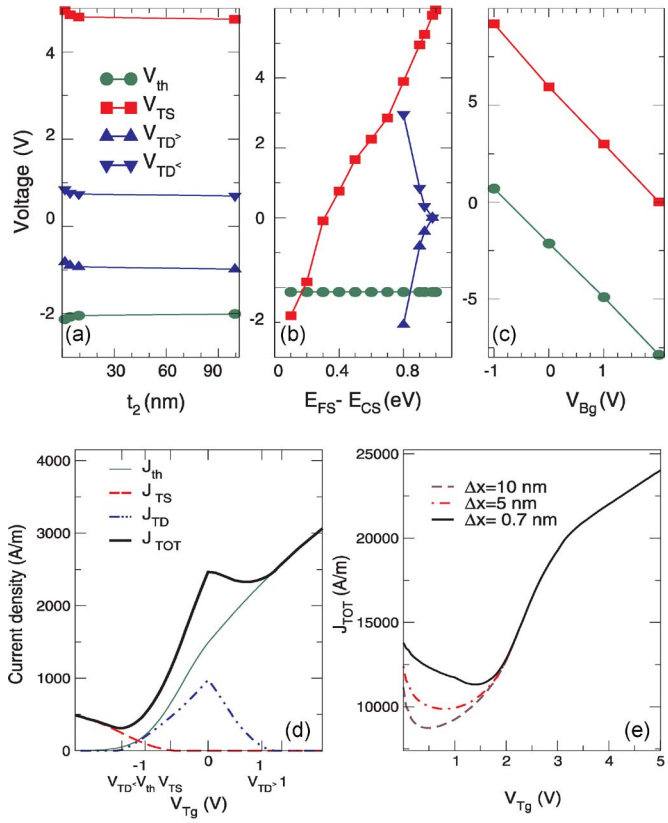

Fig. 5. (a) Thresholds as a function of the oxide thickness t_2 for $V_{\rm DS} = 0.5$ V, $V_{\rm BG} = 0$ V, and $E_{\rm FS} - E_{\rm CS} = 0.9$ eV. (b) Thresholds as a function of $E_{\rm FS} - E_{\rm CS}$ for $t_2 = 1.5$ nm, $V_{\rm DS} = 0.5$ V, and $V_{\rm BG} = 0$ V. (c) Thresholds as a function of $V_{\rm Bg}$ for $t_2 = 1.5$ nm, $V_{\rm DS} = 0.5$ V, and $E_{\rm FS} - E_{\rm CS} = 1$ eV. (d) Total current $J_{\rm TOT}$ and its three components $(J_{\rm TS}, J_{\rm TD}, J_{\rm th})$ for $V_{\rm DS} = 0.1$ V, $V_{\rm Bg} = 0$ V, and $E_{\rm FS} - E_{\rm CS} = 0.5$ eV. Thresholds are shown along the coordinate axis. (e) Total current for $t_2 = 1.5$ nm, $V_{\rm DS} = 0.5$ V, $E_{\rm FS} - E_{\rm CS} = 1$ eV, $V_{\rm BG} = 0$ V, and different Δx values.

$V_{\rm DS}$ ($V_{\rm DS} > 0.2$ V), where the parabolic band approximation misses to reproduce band behavior for large k_y. In Fig. 4(c), the energy gap is shown as a function of $V_{\rm Tg}$. As can be seen, even for large $V_{\rm Tg}$, the biggest attainable $E_{\rm gap}$ is close to 0.15 eV.

Let us now consider the different contributions of the three current components ($J_{\rm th}$, $J_{\rm TS}$, and $J_{\rm TD}$) to the total current $J_{\rm TOT}$ [Fig. 5(d)]. For each of these components, we can define a sort of threshold voltage, above which their contribution is not negligible. In particular, $J_{\rm th}$ starts to be relevant as soon as $E_c \sim E_{\rm FS}$. We then define $V_{\rm th}$ as the $V_{\rm Tg}$ for which $E_c = E_{\rm FS}$. Similarly, interband current $J_{\rm TS}$ is not zero when $E_v \geq E_{\rm CS}$; therefore, we define $V_{\rm TS}$ as the top-gate voltage for which $E_v = E_{\rm CS}$. Finally, $J_{\rm TD}$ is not zero in the energy range $E_{\rm CD} < E < E_{\rm VS}$: We define $V_{\rm TD}^{>}$ and $V_{\rm TD}^{<}$ as the top-gate voltages for which $E_{\rm VS} = E_{\rm CD}$; owing to these definitions, we can qualitatively evaluate current contribution by observing the band structure.

Our goal is indeed to obtain the largest value for the $I_{\rm on}/I_{\rm off}$ ratio, and this is only possible if the band-to-band component of the current is suppressed. We have considered three different solutions to accomplish this task: by varying the back-gate oxide (t_2), by varying the $E_{\rm FS} - E_{\rm CS}$ or $E_{\rm FD} - E_{\rm CD}$ difference, or by simply varying the back-gate voltage. If otherwise specified, $\Delta x = 0.7$ nm, as obtained from TB simulations of

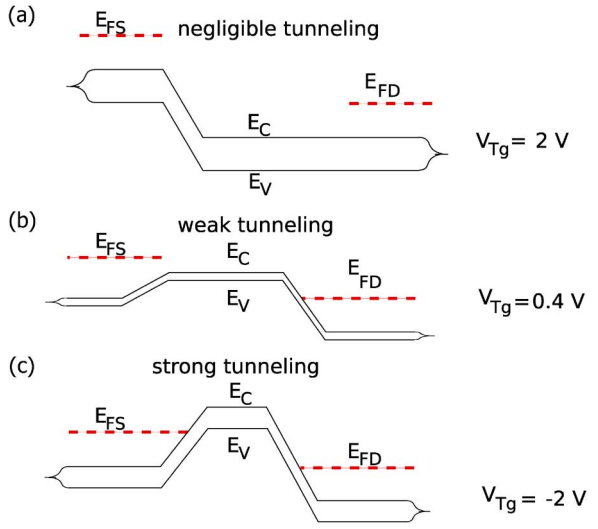

Fig. 6. Simulated band edges when (a) tunnel current weakly affects $J_{\rm TOT}$, (b) $J_{\rm TS}+J_{\rm TD}$ is one order of magnitude smaller than the total current, and (c) interband tunneling current is the dominant component.

an abrupt junction with the same doping of the considered BG-FET. In Fig. 5(a)–(c), the previously defined thresholds are shown for the three considered cases.

As shown in Fig. 5(a), back-gate oxide thickness has no effect in our case, since the top layer screens the electric field induced by the top gate, as also shown in Fig. 4(b), where V_2 remains almost constant. Fig. 5(b) shows thresholds as a function of $(E_{\rm FS}-E_{\rm CS})$ and, therefore, as a function of dopant concentration. We observe that, for $E_{\rm FS}-E_{\rm CS}=1$ eV, $V_{\rm TD}^{>}=V_{\rm TD}^{<}$, so that $J_{\rm TD}$ is practically eliminated, while $J_{\rm TS}$ increases since $V_{\rm TS}$ becomes larger. In Fig. 5(c), we show $V_{\rm th}$ and $V_{\rm TS}$, for $E_{\rm FS}-E_{\rm CS}=1$ eV, as a function of $V_{\rm Bg}$. Unfortunately, the two curves have the same behavior, so that $V_{\rm TS}$ cannot be reduced to values smaller than $V_{\rm th}$, or—in other words—we cannot suppress current due to interband tunneling at source contact.

We have then computed the transfer characteristics for $V_{\rm Bg}=0$ V, $t_1=t_2=1.5$ nm, and $E_{\rm FS}-E_{\rm CS}=1$ eV. In Fig. 5(e), $J_{\rm TOT}$ is shown. As can be seen, poor $I_{\rm on}/I_{\rm off}$ ratio can be obtained since band-to-band tunneling at source contact is too high as also observed in graphene FETs [30]. Reducing $\mathcal{E}$, i.e., $T(k_y)$, could lead to a reduction of $J_{\rm TS}$ and, consequently, to an improvement of the $I_{\rm on}/I_{\rm off}$ ratio. As shown in Fig. 5(e), an improved $I_{\rm on}/I_{\rm off}$ is obtained by increasing Δx to 5–10 nm, but it is still lower than the ITRS requirements (10^4) for digital circuits. In Fig. 6, we also sketch the simulated band edges for three different cases: 1) when tunneling is negligible ($J_{\rm TOT}\simeq J_{\rm Ti}$ for $V_{\rm Tg}=2$ V); 2) when tunneling weakly affects the total current ($J_{\rm TOT}\simeq 10(J_{\rm TS}+J_{\rm TD})$ for $V_{\rm Tg}=0.4$ V); and 3) when tunneling represents the predominant component ($J_{\rm TOT}\simeq(J_{\rm TS}+J_{\rm TD})$ for $V_{\rm Tg}=-2$ V).

IV. Conclusion

We have developed an analytical model for BG-FETs, suitable for the exploration of the design parameter space. The model is based on some simplifying assumptions, such as the effective mass approximation, but includes all the relevant physics of bilayer graphene. First and foremost, it includes the tunable gap of bilayer graphene with the vertical electric field, which is exploited in order to induce the largest gap, when the device is in the OFF state. It also fully includes polarization of bilayer graphene in response to a vertical electric field. As far as transport is concerned, it includes the thermionic current components and all interband tunneling components, which are the main limiting factors in achieving a large $I_{\rm on}/I_{\rm off}$ ratio. Significant aspects of the model have been validated through comparisons with numerical TB NEGF simulations.

Due to the small computational requirements, we have been able to explore the parameter design space of bilayer-graphene FETs in order to maximize the $I_{\rm on}/I_{\rm off}$ ratio. Despite applied vertical field manages to induce an energy gap on the order of 100 meV, band-to-band tunneling greatly affects device performance, limiting its use for device applications. A larger gap must be induced to make bilayer graphene a useful channel material for digital applications, probably by combining different options, such as using bilayer graphene in addition to limited lateral confinement, stress, or doping.

Appendix A

A. Density of States

The total density of states can be computed as follows, performing the integral over the first Brillouin zone (BZ):

$$D(E)=\frac{2}{(2\pi)^2}\int_{\rm BZ}\delta\left(E_c+\frac{\hbar^2}{2m^*}\left(|\mathbf{k}|-k_{\rm min}\right)^2-E\right)2\pi k dk. \tag{20}$$

If we apply the following property of the delta function:

$$\delta\left[f(x)\right]=\sum_n\frac{\delta(x-x_n)}{|f'(x_n)|} \tag{21}$$

where x_n are the zeroes of the function $f(x)$, (20) reads

$$\begin{aligned}D(E)&=\frac{1}{\pi}\frac{\sqrt{2m^*}}{\hbar}\frac{1}{2\sqrt{E-E_c}}\int_{\rm BZ'}\delta(r-\sqrt{E-E_c})\\&\quad\times\left(\frac{\sqrt{2m^*}}{\hbar}r+k_{\rm min}\right)dr\\&=\frac{1}{2\pi\hbar}\left(\frac{2m^*}{\hbar}+\sqrt{\frac{2m^*}{E-E_c}}k_{\rm min}\right)\end{aligned} \tag{22}$$

where $\mathrm{r}=(\hbar/\sqrt{2m^*})(|\mathbf{k}|-k_{\rm min})$.

B. Thermionic Current

In order to derive the expression of the thermionic current, first, we have to compute the group velocity v_x, which reads

$$\begin{aligned}\frac{1}{\hbar}\frac{\partial E(k_x,k_y)}{\partial k_x}&=\frac{\mathbf{1}}{\hbar}\frac{\partial}{\partial k_x}\left(\frac{E_{\rm gap}}{2}+\frac{\hbar^2}{2m^*}\left(|\mathbf{k}|-k_{\rm min}\right)^2\right)\\&=\frac{\hbar k_x}{m^*}\left(1-\frac{k_{\rm min}}{|\mathbf{k}|}\right).\end{aligned} \tag{23}$$

Replacing (23) in (16), we obtain

$$J_{\rm th} = \frac{-q\hbar}{\pi^2 m^*} \int_{-\infty}^{+\infty} dk_y \left[\int_{k_x^>} k_x \left(1 - \frac{k_{\rm min}}{|\mathbf{k}|}\right) f(E - E_{\rm FS}) dk_x + \int_{k_x^<} k_x \left(1 - \frac{k_{\rm min}}{|\mathbf{k}|}\right) f(E - E_{\rm FD}) dk_x \right]. \tag{24}$$

In order to remove the singularity in (24) for $k_x = k_y = 0$, we can use cylindrical coordinates, i.e., $k_x = k\cos\theta$, $k_y = k\sin\theta$, and $|\mathbf{k}| = k$. In this representation, the condition $v_x > 0$ translates in

$$\begin{cases} k\cos\theta > 0 \\ k - k_{\rm min} > 0 \end{cases} \qquad \begin{cases} k\cos\theta < 0 \\ k - k_{\rm min} < 0. \end{cases}$$

The integral (24) becomes

$$J_{\rm th} = \frac{2q\hbar}{\pi^2 m^*} \int_0^{k_{\rm max}} k(k - k_{\rm min}) \left[f_S(E,k) - f_D(E,k) \right] dk. \tag{25}$$

C. Transmission Coefficient

The tunneling transmission probability $T(k_y)$ has been computed through the WKB approximation. The $|{\rm Im}\{k_x\}|$ in (18) is computed from the energy dispersion relation as follows: From (19), we can write

$$\left(\sqrt{k_x^2 + k_y^2} - k_{\rm min}\right)^2 = \frac{2m^*}{\hbar^2}\left(q\mathcal{E}x - \frac{E_{\rm gap}}{2}\right). \tag{26}$$

Defining

$$\beta(x) = \frac{\sqrt{2m^*\left(\frac{E_{\rm gap}}{2} - q\mathcal{E}x\right)}}{\hbar} > 0 \tag{27}$$

and inserting (27) in (26), we obtain

$$\left(k_x^2 + k_y^2\right)^{\frac{1}{2}} - k_{\rm min} = i\beta(x) \tag{28}$$

which reads

$$k_x^2 = \left(k_{\rm min}^2 - \beta(x)^2 - k_y^2\right) + 2i\beta(x)k_{\rm min}. \tag{29}$$

If we expressed k_x as $k_x = a + ib (a, b \in \Re)$, k_x^2 reads

$$k_x^2 = a^2 - b^2 + 2iab. \tag{30}$$

By comparing (29) and (30), $|{\rm Im}\{k_x\}|$ simply reads

$$|{\rm Im}\{k_x\}| = \sqrt{\frac{C + \sqrt{C^2 + 4\beta(x)^2 k_{\rm min}^2}}{2}} \tag{31}$$

with $C = -k_{\rm min}^2 + \beta^2(x) + k_y^2$.

ACKNOWLEDGMENT

The authors would like to thank the Network for Computational Nanotechnology for providing the computational resources at nanohub.org, through which part of the results shown in this paper has been obtained.

REFERENCES

[1] International Technology Roadmap for Semiconductor, 2007. [Online]. Available: http://public.itrs.net
[2] Z. F. Wang, H. Zheng, Q. W. Shi, and J. Chen, "Emerging nanocircuit paradigm: Graphene-based electronics for nanoscale computing," in *Proc. IEEE NANOARCH*, Oct. 2007, pp. 93–100.
[3] S. Iijima, "Helical microtubules of graphitic carbon," *Nature*, vol. 354, no. 6348, pp. 56–58, Nov. 1991.
[4] K. S. Novoselov, A. K. Geim, S. V. Morozov, D. Jiang, Y. Zhang, S. V. Dubonos, I. V. Grigorieva, and A. A. Firsov, "Electric field effect in atomically thin carbon films," *Science*, vol. 306, no. 5696, pp. 666–669, Oct. 2004.
[5] A. H. C. Neto, F. Guinea, N. M. R. Peres, K. S. Novoselov, and A. K. Geim, "The electronic properties of graphene," *Rev. Mod. Phys.*, vol. 81, no. 1, pp. 109–163, Jan. 2009.
[6] A. K. Geim and K. S. Novoselov, "The rise of graphene," *Nat. Mater*, vol. 6, no. 3, pp. 183–191, Mar. 2007.
[7] K. S. Novoselov, A. K. Geim, S. V. Morozov, D. Jiang, M. I. Katsnelson, I. V. Grigorieva, S. V. Dubonos, and A. A. Firsov, "Two-dimensional gas of massless Dirac fermions in graphene," *Nature*, vol. 438, no. 7065, pp. 197–200, Nov. 2005.
[8] V. P. Gusynin and S. G. Sharapov, "Unconventional integer quantum hall effect in graphene," *Phys. Rev. Lett.*, vol. 95, no. 14, pp. 146 801–146 805, Sep. 2005.
[9] J. C. Meyer, A. K. Geim, M. I. Katsnelson, K. S. Novoselov, T. J. Booth, and S. Roth, "The structure of suspended graphene sheets," *Nature*, vol. 446, no. 7131, pp. 60–63, Dec. 2006.
[10] J. S. Bunch, A. M. Van der Zande, S. S. Verbridge, I. W. Frank, D. M. Tanenbaum, J. M. Parpia, H. G. Craighead, and P. L. McEuen, "Electromechanical resonators from graphene sheets," *Science*, vol. 315, no. 5811, pp. 490–493, Jan. 2007.
[11] D. A. Dikin, S. Stankovich, E. J. Zimney, R. D. Piner, G. H. B. Dommett, G. Evmenenko, S. T. Nguyen, and R. S. Ruoff, "Preparation and characterization of graphene oxide paper," *Nature*, vol. 448, no. 7152, pp. 457–460, Jul. 2007.
[12] G. Fiori and G. Iannaccone, "Simulation of graphene nanoribbon field-effect transistors," *IEEE Electron Device Lett.*, vol. 28, no. 8, pp. 760–762, Aug. 2007.
[13] C. Zhou, J. Kong, and H. Dai, "Electrical measurements of individual semiconducting single-walled nanotubes of various diameters," *Appl. Phys. Lett.*, vol. 76, no. 12, pp. 1597–1599, Mar. 2000.
[14] Z. Chen, Y.-M. Lin, M. J. Rooks, and P. Avouris, "Graphene nano-ribbon electronics," *Physica E*, vol. 40, no. 2, pp. 228–232, Jun. 2007.
[15] Y.-W. Son, M. L. Cohen, and S. G. Louie, "Energy gaps in graphene nanoribbons," *Phys. Rev. Lett.*, vol. 97, no. 21, pp. 216 803–216 806, Nov. 2006.
[16] M. Y. Han, B. Özyilmaz, Y. Zhang, and P. Kim, "Energy band-gap engineering of graphene nanoribbons," *Phys. Rev. Lett.*, vol. 98, no. 20, pp. 206 805–206 809, May 2007.
[17] J. Nilsson, C. A. H. Neto, F. Guinea, and N. M. R. Peres, "Electronic properties of bilayer and multilayer graphene," *Phys. Rev. B, Condens. Matter*, vol. 78, no. 4, pp. 045405-1–045405-34, Jul. 2008.
[18] E. V. Castro, K. S. Novoselov, S. V. Morozov, N. M. R. Peres, J. M. B. L. dos Santos, J. Nilsson, F. Guinea, A. K. Geim, and A. H. C. Neto, "Biased bilayer graphene: Semiconductor with a gap tunable by the electric field effect," *Phys. Rev. Lett.*, vol. 99, no. 21, p. 216 802, Nov. 2007.
[19] E. McCann, "Asymmetry gap in the electronic band structure of bilayer graphene," *Phys. Rev. B, Condens. Matter*, vol. 74, no. 16, pp. 161 403–161 407, Nov. 2006.
[20] T. Ohta, A. Bostwick, T. Seyller, K. Horn, and E. Rotenberg, "Controlling the electronic structure of bilayer graphene," *Science*, vol. 313, no. 5789, pp. 951–954, Aug. 2006.
[21] Y. Ouyang, P. Campbell, and J. Guo, "Analysis of ballistic monolayer and bilayer graphene field-effect transistors," *Appl. Phys. Lett.*, vol. 92, no. 92, pp. 063120–063122, Feb. 2008.

[22] N. Harada, M. Ohfuti, and Y. Awano, "Performance estimation of graphene field-effect-transistors using semiclassical Monte Carlo simulation," *Appl. Phys. Exp.*, vol. 1, no. 1, pp. 024002–024004, Feb. 2008.
[23] G. Fiori and G. Iannaccone, "On the possibility of tunable-gap bilayer graphene FET," *IEEE Electron Device Lett.*, vol. 30, no. 3, pp. 261–264, Mar. 2009.
[24] V. Ryzhii, M. Ryzhii, A. Satou, T. Otsuji, and N. Kirova, "Device model for graphene bilayer field-effect transistor," *J. Appl. Phys.*, vol. 105, no. 10, p. 104 510, Dec. 2009.
[25] Nanotcad Vides. [Online]. Available: http://www.nanohub.org/tools/vides
[26] K. Natori, "Ballistic metal–oxide–semiconductor field effect transistor," *J. Appl. Phys.*, vol. 76, no. 8, pp. 4879–4890, Jul. 1994.
[27] P. R. Wallace, "The band theory of graphite," *Phys. Rev.*, vol. 71, no. 9, pp. 622–634, May 1947.
[28] X. Li, X. Wang, L. Zhang, S. Lee, and H. Dai, "Chemically derived, ultrasmooth graphene nanoribbon semiconductors," *Science*, vol. 319, no. 5867, pp. 1229–1232, Feb. 2008.
[29] J. W. G. Wildoer, L. C. Venema, A. G. Rinzler, R. E. Smalley, and C. Dekker, "Electronic structure of atomically resolved carbon nanotubes," *Nature*, vol. 391, no. 6662, pp. 59–62, Jan. 1998.
[30] V. Ryzhii, M. Ryzhii, and T. Otsuji, "Thermionic and tunneling transport mechanism in graphene field-effect transistors," *Phys. Stat. Sol. (A)*, vol. 205, no. 7, pp. 1527–1533, Mar. 2008.

Martina Cheli received the M.S. degree in physics from the Università di Pisa, Pisa, Italy, in 2007, where she is currently working toward the Ph.D. degree in the Dipartimento di Ingegneria dell'Informazione: Elettronica, Informatica, Telecomunicazioni.

Her main research activity concerns the analytical modeling and the simulation of novel nanoelectronic devices based on graphene.

Gianluca Fiori received the M.S. degree in electrical engineering and the Ph.D. degree from the Università di Pisa, Pisa, Italy, in 2001 and 2005, respectively.

In the autumn of 2002, he visited Silvaco International, developing quantum models, which are currently implemented in the commercial simulator ATLAS by Silvaco. In the summer of 2004, 2005, and 2008, he was with Purdue University, West Lafayette, IN, where he worked on models for the simulation of transport in nanoscaled devices. Since December 2007, he has been an Assistant Professor with the Dipartimento di Ingegneria dell'Informazione: Elettronica, Informatica, Telecomunicazioni, Università degli Studi di Pisa. His main field of activity includes the development of models and codes for the simulations of ultrascaled semiconductor devices.

Giuseppe Iannaccone (M'98) received the M.S.E.E. and Ph.D. degrees in electrical engineering from the Università di Pisa, Pisa, Italy, in 1992 and 1996, respectively.

In 1996, he took a permanent position as a Researcher with the Italian National Research Council, and in the same year, he obtained a faculty position with the Dipartimento di Ingegneria dell'Informazione: Elettronica, Informatica, Telecomunicazioni, Università di Pisa, first, as Assistant Professor, and then, since January 2001, as Associate Professor of Electronics. He is strongly involved in the activities of the Technology Transfer Office of the university and is a Founder of the Università di Pisa spin-off company Quantavis s.r.l. He has coordinated a few European and National projects involving multiple partners and has acted as Principal Investigator in several research projects funded by public agencies at the European and national levels and by private organizations. He has authored and coauthored more than 120 papers published in peer-reviewed journals and more than 80 papers in proceedings of international conferences. He is a Referee for leading journals in the fields of condensed matter physics, device electronics, and circuit design. His interests include transport and noise in nanoelectronic and mesoscopic devices, development of device modeling and TCAD tools, and the design of extremely low power circuits and systems for RFID and ambient intelligence scenarios.